Cen Xie,[1] Changtao Jiang,[2,3] Jingmin Shi,[1] Xiaoxia Gao,[1] Dongxue Sun,[1] Lulu Sun,[2,3] Ting Wang,[2,3] Shogo Takahashi,[1] Mallappa Anitha,[4] Kristopher W. Krausz,[1] Andrew D. Patterson,[4] and Frank J. Gonzalez[1]

An Intestinal Farnesoid X Receptor–Ceramide Signaling Axis Modulates Hepatic Gluconeogenesis in Mice

Diabetes 2017;66:613–626 | DOI: 10.2337/db16-0663

Increasing evidence supports the view that intestinal farnesoid X receptor (FXR) is involved in glucose tolerance and that FXR signaling can be profoundly impacted by the gut microbiota. Selective manipulation of the gut microbiota–FXR signaling axis was reported to significantly impact glucose intolerance, but the precise molecular mechanism remains largely unknown. Here, caffeic acid phenethyl ester (CAPE), an over-the-counter dietary supplement and an inhibitor of bacterial bile salt hydrolase, increased levels of intestinal tauro-β-muricholic acid, which selectively suppresses intestinal FXR signaling. Intestinal FXR inhibition decreased ceramide levels by suppressing expression of genes involved in ceramide synthesis specifically in the intestinal ileum epithelial cells. The lower serum ceramides mediated decreased hepatic mitochondrial acetyl-CoA levels and pyruvate carboxylase (PC) activities and attenuated hepatic gluconeogenesis, independent of body weight change and hepatic insulin signaling in vivo; this was reversed by treatment of mice with ceramides or the FXR agonist GW4064. Ceramides substantially attenuated mitochondrial citrate synthase activities primarily through the induction of endoplasmic reticulum stress, which triggers increased hepatic mitochondrial acetyl-CoA levels and PC activities. These results reveal a mechanism by which the dietary supplement CAPE and intestinal FXR regulates hepatic gluconeogenesis and suggest that inhibiting intestinal FXR is a strategy for treating hyperglycemia.

Enhanced hepatic gluconeogenesis contributes to hyperglycemia in type 2 diabetes (1). Pyruvate carboxylase (PC) expression is positively correlated with fasting hyperglycemia with liver-specific PC inhibition preventing high-fat diet (HFD)–induced obesity, hepatic steatosis, and glucose intolerance (2). PC activation is positively regulated by acetyl-CoA in the liver (3), and hepatic acetyl-CoA is a key metabolic intermediate that regulates hepatic gluconeogenesis independent of hepatic insulin signaling (4).

Bile acids, including chenodeoxycholic acid (CDCA), deoxycholic acid, and lithocholic acid, are endogenous farnesoid X receptor (FXR) activators (5). Hepatic FXR activation by the FXR synthetic agonist GW4064 restores glucose intolerance and insulin resistance (6). In addition, the conjugated bile acid tauro-β-muricholic acid (T-β-MCA) was found to be a natural FXR antagonist in mice (7,8), and increased intestinal T-β-MCA levels ameliorate HFD-induced obesity, glucose intolerance, and hepatic steatosis via inhibition of intestinal FXR signaling (8,9). However, the molecular mechanism by which intestinal FXR inhibition restores HFD-disrupted glucose homeostasis is poorly understood and the subject of the current study. Although T-β-MCA is a natural FXR antagonist produced in liver, it is rapidly hydrolyzed into β-MCA by bacterial bile salt hydrolase (BSH) in the gut (9), resulting in levels that are too low in the intestine to inhibit FXR signaling. Therefore, inhibition of bacterial BSH could block intestinal FXR signaling by increasing intestinal T-β-MCA. To this end, treatment

[1]Laboratory of Metabolism, Center for Cancer Research, National Cancer Institute, National Institutes of Health, Bethesda, MD
[2]Department of Physiology and Pathophysiology, School of Basic Medical Sciences, Peking University, Beijing, China
[3]Key Laboratory of Molecular Cardiovascular Science, Ministry of Education, Beijing, China
[4]Center for Molecular Toxicology and Carcinogenesis, Department of Veterinary and Biomedical Sciences, The Pennsylvania State University, University Park, PA
Corresponding authors: Frank J. Gonzalez, gonzalef@mail.nih.gov, and Changtao Jiang, jiangchangtao@bjmu.edu.cn.

Received 25 May 2016 and accepted 29 October 2016.
This article contains Supplementary Data online at http://diabetes.diabetesjournals.org/lookup/suppl/doi:10.2337/db16-0663/-/DC1.

See accompanying article, p. 571.

with caffeic acid phenethyl ester (CAPE), a BSH inhibitor (10), was used in the current study. BSH increased T-β-MCA, resulting in inhibition of intestinal FXR signaling and decreased ceramide synthesis. Decreased ceramides lowered hepatic mitochondrial acetyl-CoA levels and PC activities and attenuated hepatic gluconeogenesis.

RESEARCH DESIGN AND METHODS

Materials and Reagents

CAPE was purchased from Bachem Americas, Inc. (Torrance, CA). GW4064 was purchased from Selleck Chemicals (Houston, TX). Bile acids were purchased from Steraloids, Inc. (Newport, RI) and Sigma-Aldrich (St. Louis, MO), and T-CDCA-d5 sodium salt and CDCA-d5 were purchased from Toronto Research Chemicals, Inc. (Toronto, Ontario). Glucose, pyruvate, citrate, α-ketoglutarate, succinate, fumarate, malate, and thapsigargin were obtained from Sigma-Aldrich. C2:0, C16:0, C18:0, C20:0, C22:0, C24:0, and C24:1 ceramides were purchased from Avanti Polar Lipids (Alabaster, AL). HFD (60% kcal from fat) was obtained from Bio-Serv, Inc. (Frenchtown, NJ).

Animal Studies

Male mice are more sensitive to diet-induced obesity and diabetes than female mice, and thus male mice were used in this study. Six- to eight-week-old male littermate $Fxr^{fl/fl}$ and $Fxr^{\Delta IE}$ mice (11) were fed an HFD and gavaged with vehicle or CAPE (75 mg/kg/day) for 4 weeks. For the GW4064 and ceramide turnover study, male C57BL/6N mice fed an HFD were gavaged with vehicle, CAPE (75 mg/kg/day), or GW4064 (10 mg/kg/day) + CAPE for 4 weeks. For the short-term HFD feeding experiment, mice were fed an HFD for 1 week. For the short-term ceramide turnover study, mice fed an HFD were intraperitoneally injected with corn oil or C16:0 ceramide (10 mg/kg) for 1 week. For the endoplasmic reticulum (ER) stress inhibition study, mice fed an HFD were intraperitoneally injected with vehicle or C16:0 ceramide at a dose of 10 mg/kg/day for 1 week. Tauroursodeoxycholic acid (TUDCA) (150 mg/kg, ER stress inhibitor) or saline was intraperitoneally injected to mice at 24 and 4 h before they were killed. All of the mice were randomly assigned to experimental groups (at least five mice per group), and the groups did not present differences in body weights before the treatments. All animal studies were performed in accordance with the Institute of Laboratory Animal Resources guidelines and approved by the National Cancer Institute Animal Care and Use Committee. All mice were fed ad libitum and kept in a 12-h light-dark cycle.

Metabolic Assays

Glucose or pyruvate at 2 g/kg in saline was injected intraperitoneally in conscious animals. Fasting serum insulin levels were measured with a mouse insulin ELISA kit (Crystal Chem, Downers Grove, IL).

Primary Hepatocyte Cultures and Treatment

Primary hepatocytes were isolated as previously described (9). After starvation for 6 h, hepatocytes were exposed to C2:0 ceramide (10, 20, and 50 μmol/L) and thapsigargin (500 nmol/L, positive control, ER stress inducer) for 8 h. In certain experiments, TUDCA (1 mmol/L, ER stress inhibitor) was added 1 h before C2:0 ceramide and thapsigargin stimulation.

Hepatic Glucose Production

Cultured primary hepatocytes were incubated with serum-, glucose-, and pyruvate-free DMEM. After 1 h of incubation, TUDCA (1 mmol/L) was added. After another 1-h incubation, C2:0 ceramide (20 and 50 μmol/L), thapsigargin (500 nmol/L, positive control, ER stress inducer), and gluconeogenic substrate pyruvate (1 mmol/L) were added and incubated for an additional 4 h. The amount of glucose released in the medium was measured using a glucose kit (Abcam, Cambridge, MA).

BSH Activity Assay

Cecal proteins and BSH activity measurement were performed as previously described (8).

Determination of Pyruvate and Oxaloacetate Concentrations

The pyruvate and oxaloacetate concentrations in frozen liver samples were analyzed with a pyruvate assay kit and an oxaloacetate assay kit (Abcam). The concentration was normalized by protein content.

Quantification of Mitochondrial Acetyl-CoA Levels

Liver mitochondria were prepared using a mitochondria isolation kit (Sigma-Aldrich). Acetyl-CoA levels in mitochondria were then determined using a PicoProbe acetyl-CoA assay kit (Abcam).

Mitochondrial Citrate Synthase and PC Activity Assays

Liver citrate synthase (CS) activity was determined in the mitochondrial fraction after disruption by sonication using a synthase activity assay kit (Abcam). PC activity in the mitochondrial fraction was assayed by coupling oxaloacetate production from pyruvate by PC to NADH oxidation by malate dehydrogenase (2).

Real-Time PCR Analysis

Real-time PCR primer sequences are included in Supplementary Table 1.

Metabolomic Analysis

The global metabolomics and the lipidomics analysis were undertaken as previously described (9).

Data Analysis

When comparing two groups, statistical significance was determined using two-tailed Student *t* test. When more than two groups were investigated, one-way ANOVA followed by Tukey post hoc correction was applied for comparisons. *P* values of <0.05 were considered significant.

RESULTS

Inhibition of Intestinal FXR Is Necessary to Improve Hepatic Glucose Homeostasis by CAPE

CAPE is a potential BSH inhibitor identified by high-throughput screening in vitro (10). To verify the effects of CAPE on BSH in vivo, the cecum content BSH activities

were measured in mice on an HFD after they were subjected to CAPE treatment, which was found to substantially attenuate the BSH activities (Supplementary Fig. 1*A*). This resulted in reduced total and individual free bile acid levels in feces of CAPE-treated mice (Supplementary Fig. 1*B* and *C*), whereas both total and individual taurine-conjugated bile acid levels were substantially increased in the ileum after the CAPE treatment (Supplementary Fig. 1*D* and *E*). Notably T-β-MCA was increased in ileum and feces whereas β-MCA was decreased in feces (Supplementary Fig. 1*C* and *E*). CAPE treatment increased the percentage of T-β-MCA relative to total bile acids in ileum (Supplementary Fig. 1*F*), while hepatic levels of taurocholic acid (TCA), T-α-MCA, and T-β-MCA were slightly increased, and serum levels of taurine-conjugated bile acids remained similar after CAPE treatment (Supplementary Fig. 1*G* and *H*).

CAPE treatment suppressed ileum FXR signaling, as shown by decreased expression of mRNAs encoded by the FXR target genes *Shp*, *Fgf15, Osta*, and *Ostb* in ileum, but no changes in expression were found in liver (Supplementary Fig. 2*A* and *B*). The inhibition of ileum FXR signaling likely occurred due to increased T-β-MCA, an FXR antagonist (7,8), relative to other endogenous bile acid FXR agonists.

Recent studies showed that CAPE, a bioactive compound derived from propolis, improves type 2 diabetes (12). To further assess the roles of the intestinal FXR in the effects of CAPE treatment on glucose metabolism, control ($Fxr^{fl/fl}$) mice and intestine-specific *Fxr* knockout ($Fxr^{\Delta IE}$) mice fed an HFD were treated with CAPE. CAPE treatment protected $Fxr^{fl/fl}$ mice from HFD-induced body weight gain, but not in $Fxr^{\Delta IE}$ mice (Fig. 1*A*). Fasting serum glucose and insulin levels were noticeably reduced in CAPE-treated $Fxr^{fl/fl}$ mice compared with vehicle-treated $Fxr^{fl/fl}$ mice. However, $Fxr^{\Delta IE}$ mice were unresponsive to the metabolic benefits of CAPE treatment (Fig. 1*B* and *C*). Glucose tolerance test (GTT) revealed that CAPE substantially ameliorated glucose intolerance in the $Fxr^{fl/fl}$ mice, whereas it did not have an effect in the $Fxr^{\Delta IE}$ mice (Fig. 1*D*). Furthermore, pyruvate tolerance tests (PTTs) showed that hepatic gluconeogenesis was markedly inhibited in CAPE-treated $Fxr^{fl/fl}$ mice and vehicle-treated $Fxr^{\Delta IE}$ mice compared with vehicle-treated $Fxr^{fl/fl}$ mice. However, no further inhibition was observed in CAPE-treated $Fxr^{\Delta IE}$ mice compared with vehicle-treated $Fxr^{\Delta IE}$ mice (Fig. 1*E*).

To further validate the effects of the intestinal FXR pathway in the amelioration of altered glucose metabolism by CAPE, the FXR agonist GW4064 was administered to CAPE-treated mice fed an HFD. GW4064 treatment substantially reversed the inhibition of ileum FXR signaling mediated by CAPE (Supplementary Fig. 3*A*). Furthermore, GTT demonstrated that the CAPE-induced improvements in glucose intolerance were eliminated by GW4064 treatment (Supplementary Fig. 3*B* and *C*). PTT showed that GW4064 treatment reversed the inhibition of hepatic gluconeogenesis in CAPE-treated mice fed an HFD (Supplementary Fig. 3*D* and *E*).

Inhibition of Intestinal FXR Signaling by CAPE Treatment Decreases Mitochondrial Acetyl-CoA Levels, Mitochondrial PC Activities, and Gluconeogenesis in Liver

To further explore the mechanism underlying CAPE-induced inhibition of hepatic glucose metabolism, UPLC-ESI-QTOFMS–based metabolomics was used to analyze the metabolites in the livers of the vehicle- and CAPE-treated mice fed an HFD. Scores scatter plot of a partial least squares-discriminant analysis (PLS-DA) model of the UPLC-ESI-QTOFMS–positive mode data from the liver extracts distinguished different metabolic profiles in the CAPE-treated mice from the vehicle-treated mice on an HFD (Fig. 2*A*). The ions leading to the separation of the vehicle- and CAPE-treated mice were identified as the TCA cycle metabolites citrate (m/z 191.0191), α-ketoglutarate (m/z 145.1040), fumarate (m/z 115.0038), and malate (m/z 133.0145) (Fig. 2*B*), and their identities confirmed by elution times and mass fragmentation patterns that matched authentic standards (Supplementary Fig. 4). The relative levels of the TCA cycle metabolites, including citrate, α-ketoglutarate, fumarate, and malate, were substantially increased by CAPE in wild-type mice but remained unaltered by CAPE in $Fxr^{\Delta IE}$ mice fed an HFD (Fig. 2*C*). CAPE treatment markedly upregulated the levels of mRNAs encoded by the genes involved in the TCA cycle, such as citrate synthase (*Cs*), isocitrate dehydrogenase 3a (*Idh3a*), isocitrate dehydrogenase 3b (*Idh3b*), and isocitrate dehydrogenase 3 g (*Idh3g*) in $Fxr^{fl/fl}$ wild-type mice, but not in $Fxr^{\Delta IE}$ mice (Fig. 2*D*). CS is the first enzyme in the TCA cycle, and it catalyzes the generation of citrate from acetyl-CoA. Hepatic mitochondrial CS activities were substantially enhanced in CAPE-treated $Fxr^{fl/fl}$ mice compared with that of vehicle-treated $Fxr^{fl/fl}$ mice, but not in CAPE-treated $Fxr^{\Delta IE}$ mice compared with that of vehicle-treated $Fxr^{\Delta IE}$ mice (Fig. 2*E*). Increased CS activities led to decreased hepatic mitochondrial acetyl-CoA concentrations in the CAPE-treated $Fxr^{fl/fl}$ mice fed an HFD, but not in $Fxr^{\Delta IE}$ mice (Fig. 2*F*). To further investigate the mechanism by which inhibition of intestinal FXR signaling and the resultant reduced hepatic mitochondrial acetyl-CoA levels markedly decreased hepatic gluconeogenesis, the expression of genes involved in hepatic gluconeogenesis, including *Pc, Pepck*, and *G6pc*, was further examined. Interestingly, *Pc, Pepck,* and *G6pc* mRNA levels were similar in CAPE-treated $Fxr^{fl/fl}$ mice, vehicle-treated $Fxr^{\Delta IE}$ mice, and CAPE-treated $Fxr^{\Delta IE}$ mice, compared with those of vehicle-treated $Fxr^{fl/fl}$ mice (Fig. 2*G*). Acetyl-CoA was reported to allosterically induce activation of PC, the first enzyme in gluconeogenesis (3). PC activity in the mitochondrial matrix was noticeably decreased by CAPE treatment of $Fxr^{fl/fl}$ mice, but not in the $Fxr^{\Delta IE}$ mice (Fig. 2*H*). PC converts pyruvate to oxaloacetate during hepatic gluconeogenesis. Thus, the levels of pyruvate and oxaloacetate in the liver were measured, revealing that CAPE treatment increased pyruvate levels and decreased oxaloacetate levels in $Fxr^{fl/fl}$ mice, but not in $Fxr^{\Delta IE}$ mice (Fig. 2*C* and *I*). Pyruvate is also converted into the acetyl-CoA via

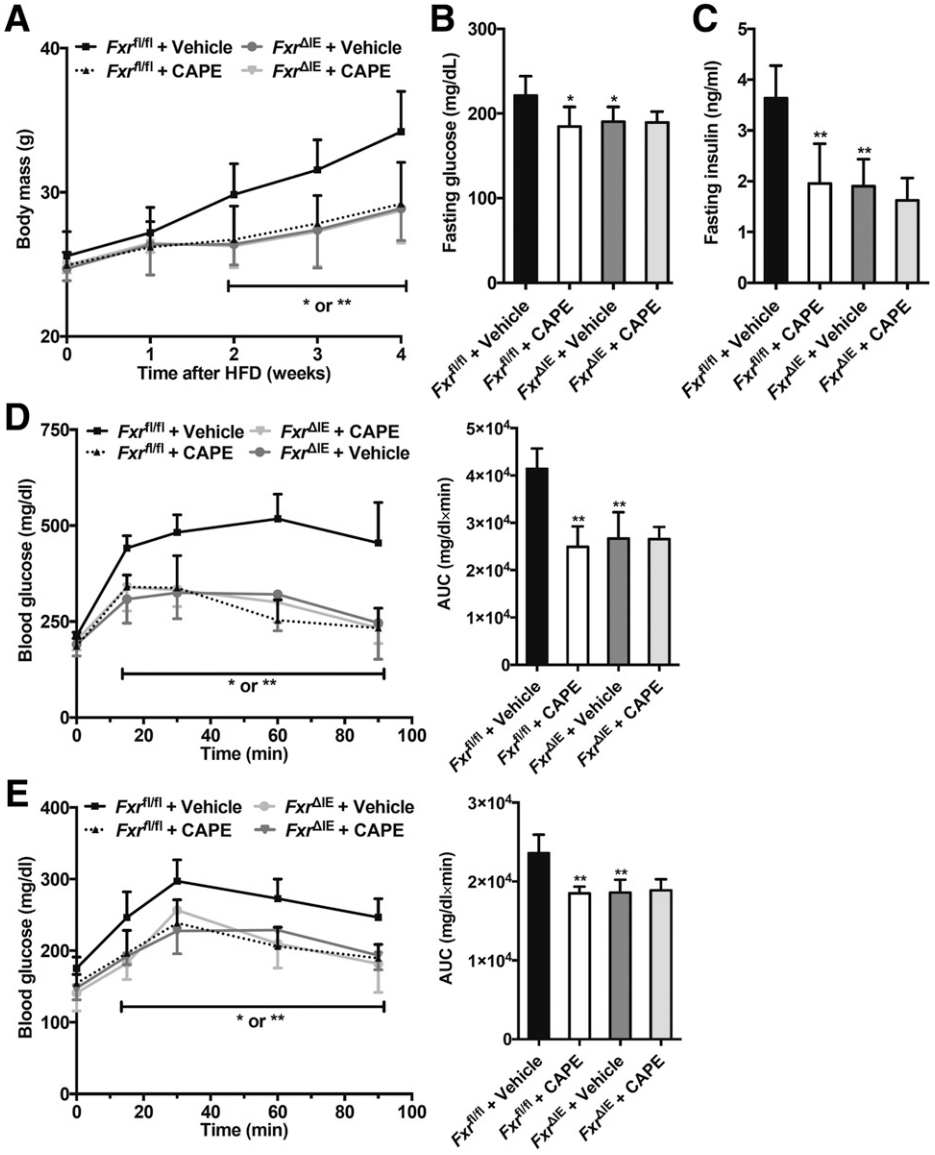

Figure 1—Inhibition of intestinal FXR mediates CAPE-induced reduction of hepatic gluconeogenesis. $Fxr^{fl/fl}$ mice and $Fxr^{\Delta IE}$ mice on an HFD were orally treated with or without CAPE for 4 weeks (n = 5). *A*: Body weights. *B*: Fasting plasma glucose levels. *C*: Fasting plasma insulin levels. *D*: GTT (left) and the area under the curve (AUC, right) at week 4. *E*: Pyruvate tolerance test (PTT, left) and AUC (right) at week 4. Data are presented as the means ± SD. One-way ANOVA with Tukey correction: $^{*}P < 0.05$ and $^{**}P < 0.01$ vs. vehicle-treated $Fxr^{fl/fl}$ mice.

oxidative decarboxylation by pyruvate dehydrogenase (PDH). PDH is inhibited by phosphorylation and activated by dephosphorylation. Although *Pdh* mRNA levels were not changed by CAPE (Fig. 2*J*), phosphorylation of PDH was reduced in $Fxr^{fl/fl}$ mice by CAPE, but not in the $Fxr^{\Delta IE}$ mice (Fig. 2*K*). These results indicated that CAPE elevated hepatic PDH activities via inhibition of intestinal FXR. Furthermore, increases in the TCA cycle metabolites citrate, α-ketoglutarate, fumarate, and malate in CAPE-treated mice were eliminated by GW4064 treatment (Fig. 3*A*). In addition, the expression of mRNAs encoded by genes related to the TCA cycle, including *Cs*, *Idh3a, Idh3b,* and *Idh3g*, that were elevated in the livers of CAPE-treated mice were reduced to control levels in the vehicle-treated group after administration of GW4064 (Fig. 3*B*). GW4064 treatment markedly reversed the CAPE-mediated increase of hepatic mitochondrial CS activities (Fig. 3*C*). The levels of hepatic mitochondrial acetyl-CoA decreased after CAPE treatment were substantially abolished by administration of GW4064 (Fig. 3*D*). Although GW4064 treatment did not affect the *Pc*, *Pepck*, and *G6pc* mRNA levels in vehicle- and CAPE-treated HFD-fed mice, the CAPE-mediated inhibition of hepatic PC activities was totally reversed by GW4064 treatment (Fig. 3*E*). The increased pyruvate levels in the livers of CAPE-treated mice were substantially blunted after administration of GW4064 (Fig. 3*F*). GW4064 treatment eliminated the CAPE-mediated inhibition of hepatic PDH

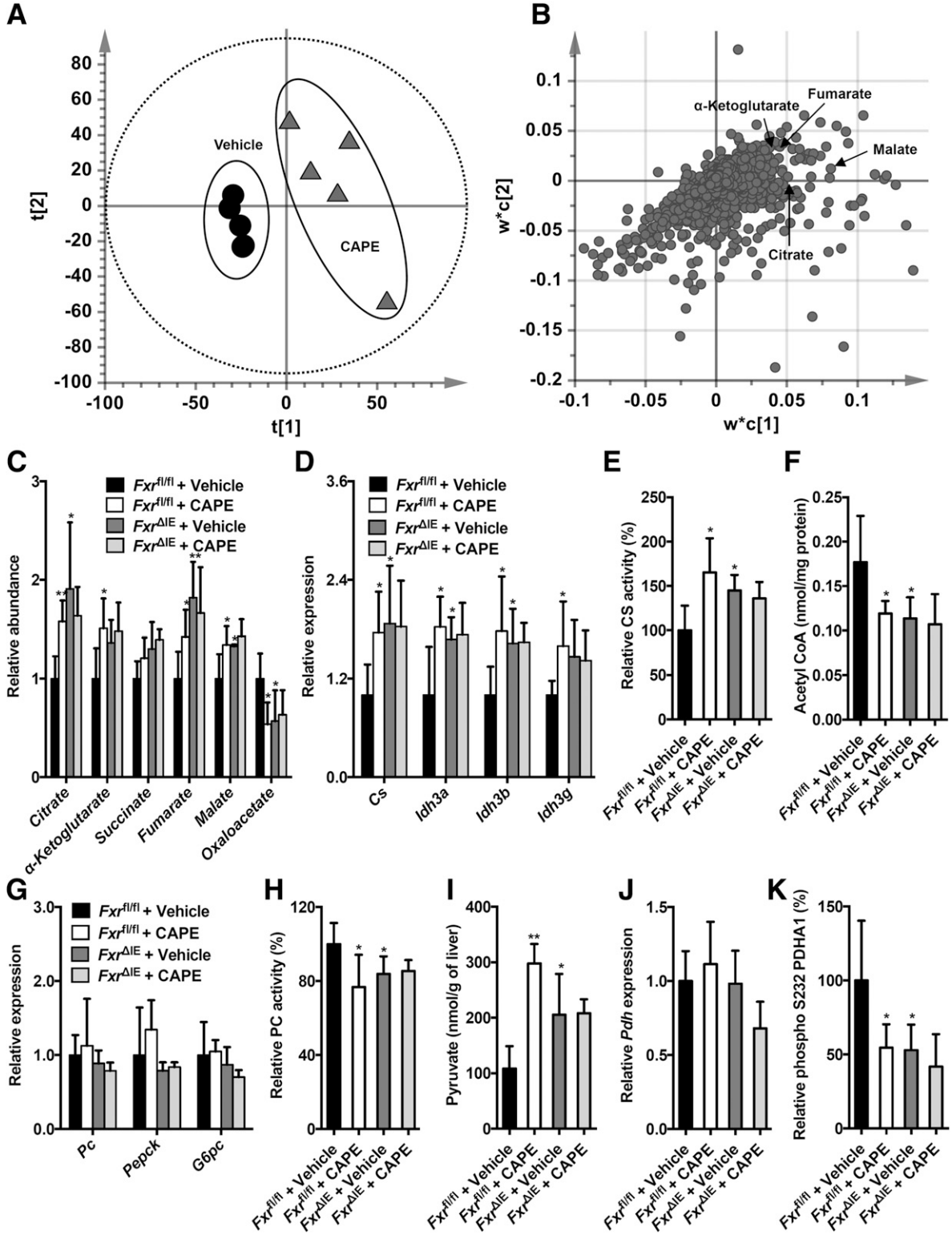

Figure 2—CAPE decreases hepatic mitochondrial acetyl-CoA and inhibits PC activities dependent on intestine FXR. Score scatter plot of a PLS-DA model of the liver ions (*A*) and loading scatter plot of a PLS-DA model of the liver ions (*B*). C57BL/6N mice on an HFD were orally treated with or without CAPE for 4 weeks (n = 5). *C*: The relative levels of TCA cycle–related metabolites. *D*: Quantitative PCR (qPCR) analysis of the hepatic expression of mRNAs encoded by the TCA cycle–related genes. *E*: The mitochondrial CS activities in the liver. *F*: The mitochondrial acetyl-CoA levels in the liver. *G*: The mRNA levels of the hepatic gluconeogenic genes. *H*: The mitochondrial PC activities in the liver. *I*: Pyruvate levels in the liver. *J*: qPCR analysis of the hepatic *Pdh* mRNA levels. *K*: The hepatic phospho-PDH activities. *C–K*: $Fxr^{fl/fl}$ mice and $Fxr^{\Delta IE}$ mice on an HFD were orally treated with or without CAPE for 4 weeks (n = 5). Data are presented as the means ± SD. One-way ANOVA with Tukey correction: $^{*}P < 0.05$ and $^{**}P < 0.01$ vs. vehicle-treated $Fxr^{fl/fl}$ mice.

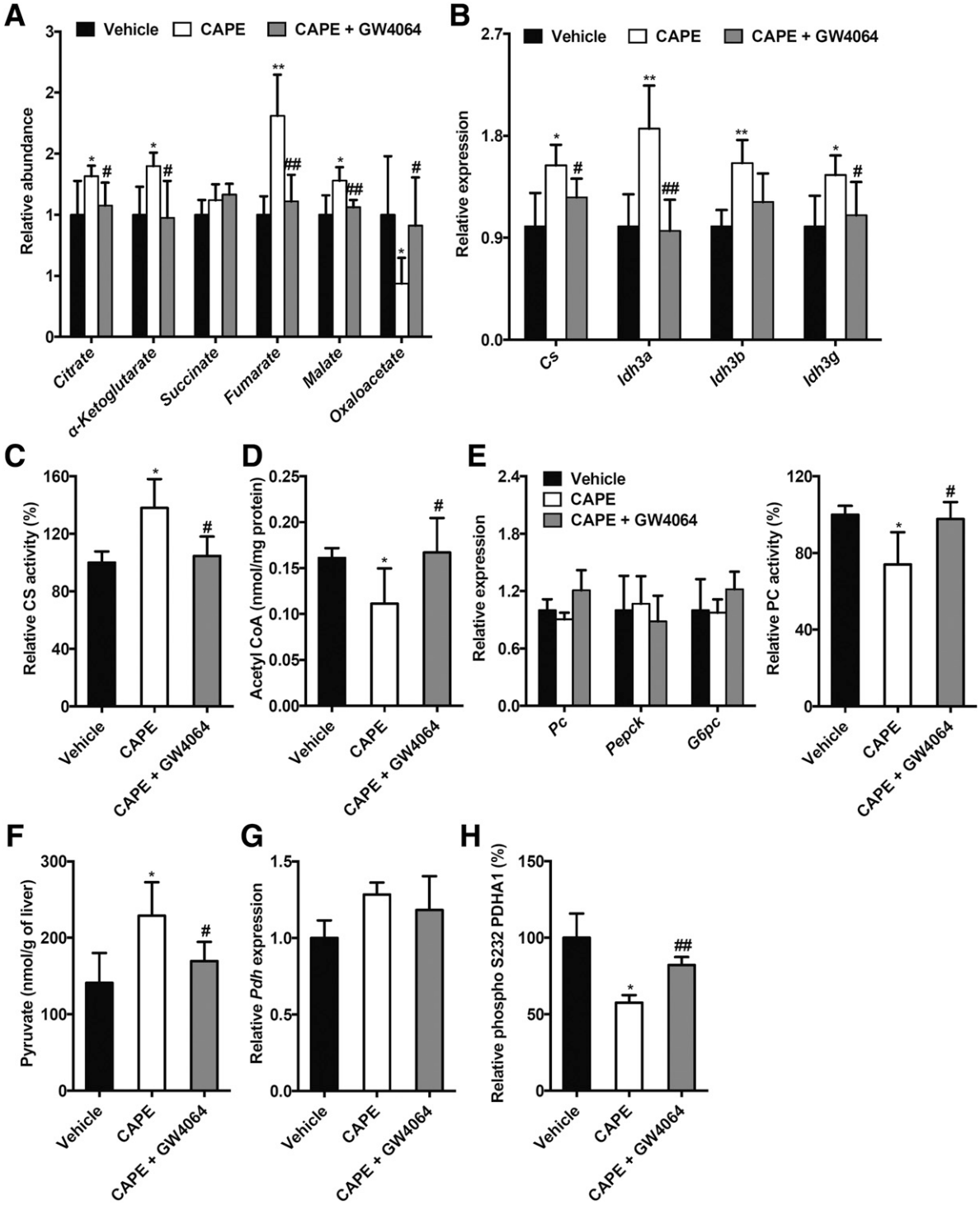

Figure 3— Downregulation of the hepatic mitochondrial acetyl-CoA levels and the PC activities by CAPE results from the inhibition of the intestinal FXR-ceramide pathway. Vehicle-, CAPE-, and CAPE+GW4064–treated mice were fed an HFD for 4 weeks (n = 5). *A*: Relative levels of TCA cycle–related metabolites in the liver. *B*: Quantitative PCR analysis of the mRNA levels of the TCA cycle–related genes in the liver. *C*: The mitochondrial CS activities in the liver. *D*: The mitochondrial acetyl-CoA levels in the liver. *E*: The mRNA levels of the hepatic gluconeogenic genes *Pepck* and *G6pc* in the liver (left). The mitochondrial PC activities in the liver (right). *F*: The hepatic pyruvate level. *G*: The hepatic *Pdh* mRNA level. *H*: The hepatic phospho-PDH activities. Data are presented as the means ± SD. One-way ANOVA with Tukey correction: *P < 0.05 and **P < 0.01 vs. vehicle; #P < 0.05 and ##P < 0.01 vs. CAPE treatment.

phosphorylation (decrease of hepatic PDH activities) but did not alter hepatic *Pdh* mRNA levels (Fig. 3*G* and *H*). Thus, the overall results indicate that CAPE substantially attenuates hepatic mitochondrial acetyl-CoA levels, PC activities, and gluconeogenesis primarily by increasing CS activities through the inhibition of intestinal FXR.

Inhibition of Intestinal FXR Signaling by CAPE Treatment Markedly Downregulates Both Intestinal and Serum Ceramide Levels

To further establish the connection between inhibition of intestinal FXR and lower hepatic gluconeogenesis after CAPE treatment in mice fed an HFD, lipidomics was carried out on serum and ileum tissue. The total and individual ceramide levels in serum and ileum were decreased in CAPE-treated HFD-fed $Fxr^{fl/fl}$ mice and vehicle-treated HFD-fed $Fxr^{\Delta IE}$ mice compared with those of vehicle-treated HFD-fed $Fxr^{fl/fl}$ mice, but no further lowering of ceramides was observed in CAPE-treated HFD-fed $Fxr^{\Delta IE}$ mice compared with that of vehicle-treated HFD-fed $Fxr^{\Delta IE}$ mice (Supplementary Fig. 5*A* and *B*). The mRNA levels of ceramide synthesis–related genes, including *Sptlc2*, *Cers2*, *Cers4*, *Degs2*, *Smpd3*, and *Smpd4*, were markedly reduced in HFD-fed $Fxr^{fl/fl}$ mice by CAPE treatment but remained unchanged in the HFD-fed $Fxr^{\Delta IE}$ mice (Supplementary Fig. 5*C* and *D*). Furthermore, decreased serum ceramides were increased to levels similar to those in the vehicle-treated group after administration of the FXR agonist GW4064 (Supplementary Fig. 5*E*). The decreased mRNA levels of *Sptlc2*, *Cers4*, *Degs2*, *Smpd3*, and *Smpd4* were also reversed by GW4064 treatment (Supplementary Fig. 5*F*).

Inhibition of the Intestinal FXR-Ceramide Pathway Decreases Hepatic Gluconeogenesis Independent of Both Body Weight and Hepatic Insulin Signaling

To further exclude decreases in body weight as a causal factor for the reduction of hepatic gluconeogenesis after the inhibition of intestinal FXR, $Fxr^{fl/fl}$ or $Fxr^{\Delta IE}$ mice were treated with an HFD or chow diet for a short duration of 1 week that does not lead to a change of body weight (Fig. 4*A*). Others have shown that treatment of mice with an HFD for only 3 days can trigger increased fasting serum glucose and glucose intolerance (13). Indeed, fasting serum glucose levels were markedly higher in $Fxr^{fl/fl}$ mice fed an HFD for 1 week than that in $Fxr^{\Delta IE}$ mice on an HFD, or $Fxr^{fl/fl}$ mice fed a chow diet (Fig. 4*B*). GTT further demonstrated that $Fxr^{\Delta IE}$ mice displayed improved glucose tolerance when on an HFD for 1 week, similar to the mice on a chow diet (Fig. 4*C* and *D*), and PTT revealed that intestine-specific *Fxr* disruption substantially suppressed hepatic gluconeogenesis to a normal level after 1 week of HFD treatment (Fig. 4*E* and *F*). Intestinal *Fxr* mRNA levels were almost absent and FXR signaling was substantially inhibited in $Fxr^{\Delta IE}$ mice compared with the $Fxr^{fl/fl}$ mice fed an HFD for 1 week (Fig. 5*A*). The expression of mRNAs encoded by *Sptlc1*, *Sptlc2*, *Cers2*, *Cers4*, *Degs2*, *Smpd1*, *Smpd3*, and *Smpd4* involved in ceramide anabolism was reduced in the $Fxr^{fl/fl}$ mice fed an HFD for 1 week (Fig. 5*B*). The $Fxr^{\Delta IE}$ mice exhibited lower ceramide levels in both serum and ileum than those of the $Fxr^{fl/fl}$ mice fed an HFD for 1 week (Fig. 5*C*). No significant alterations were observed in free fatty acid levels of the ileum and serum between the $Fxr^{fl/fl}$ and $Fxr^{\Delta IE}$ mice fed an HFD for 1 week (Fig. 4*G* and *H*). Intestine-specific FXR disruption observably enhanced hepatic mitochondrial CS activities in mice fed an HFD for 1 week (Fig. 4*I*). Hepatic mitochondrial acetyl-CoA levels and PC activities were substantially suppressed in the $Fxr^{\Delta IE}$ mice compared with those of the $Fxr^{fl/fl}$ mice fed an HFD for 1 week (Fig. 4*J* and *K*). Insulin signaling was further investigated in the liver, revealing that $Fxr^{\Delta IE}$ mice did not exhibit improved hepatic insulin signaling, as indicated by no change in insulin-induced AKT Ser473 phosphorylation (Fig. 5*D*). These results suggest that intestinal FXR orchestrates hepatic gluconeogenesis independent of both body weight and hepatic insulin signaling.

To further evaluate the roles of intestine-derived ceramide in intestinal FXR-regulated hepatic gluconeogenesis, ceramide was administered to the $Fxr^{fl/fl}$ or $Fxr^{\Delta IE}$ mice fed an HFD for a short duration (1 week). Serum ceramide levels in the $Fxr^{\Delta IE}$ mice were replenished to levels comparable to $Fxr^{fl/fl}$ mice after ceramide administration (Fig. 6*A*). Administration of ceramide markedly eliminated the decrease of fasting serum glucose levels in the $Fxr^{\Delta IE}$ mice compared with that of the $Fxr^{fl/fl}$ mice fed an HFD for 1 week, with no effect on body weight (Fig. 6*B* and *C*). GTT and PTT showed that the response to glucose and pyruvate challenge in $Fxr^{\Delta IE}$ mice was observably blunted after 1 week of ceramide treatment in mice on an HFD (Fig. 6*D* and *E*). The increased hepatic mitochondrial CS activities in the $Fxr^{\Delta IE}$ mice compared with that of the $Fxr^{fl/fl}$ mice fed an HFD for 1 week were reversed by ceramide treatment (Fig. 6*F*). The intestinal-specific FXR disruption-mediated inhibition of hepatic mitochondrial acetyl-CoA levels and PC activities was observably abolished by ceramide administration to mice fed an HFD for 1 week (Fig. 6*G* and *H*).

Ceramides Suppress Mitochondrial CS Activities by Increasing ER Stress, ER-Mitochondria Coupling, and Calcium Overload

HFD treatment was recently reported to trigger ER stress, excessive ER-mitochondria coupling, and disturbed hepatic glucose metabolism (14). Inhibition of FXR by CAPE treatment substantially inhibited the expression of hepatic mRNAs encoded by the *Bip*, *Chop*, *Vdac1*, *Pacs2*, *Ip3r1*, and *Ip3r2* genes in $Fxr^{fl/fl}$ mice but did not further inhibit beyond what was achieved in $Fxr^{\Delta IE}$ mice fed an HFD for 4 weeks (Fig. 7*A*). The downregulation of hepatic *Atf6*, *Bip*, *Chop*, *Vdac1*, *Pacs2*, *Mfn2*, and *Ip3r1* mRNAs mediated by CAPE was abolished by administration of GW4064 in mice fed an HFD for 4 weeks (Fig. 7*B*). More importantly, ceramide treatment reversed the deceased *Atf4*, *Bip*, *Chop*, *Vdac1, Pacs2*, *Mfn2*, *Ip3r1*, and *Ip3r2* mRNA levels in livers of $Fxr^{\Delta IE}$ mice compared with those of the $Fxr^{fl/fl}$ mice fed an HFD for 1 week (Fig. 7*C*). Ceramide treatment substantially enhanced the expression of mRNAs encoded by genes involved in ER stress, including *Atf4*, *Atf6*, *Bip*, and *Chop*, the related ER-mitochondria tethering genes *Pacs2* and *Mfn2*, and calcium transport–related genes *Ip3r1* and *Ip3r2* in primary hepatocytes in a dose-dependent manner (Fig. 7*D*).

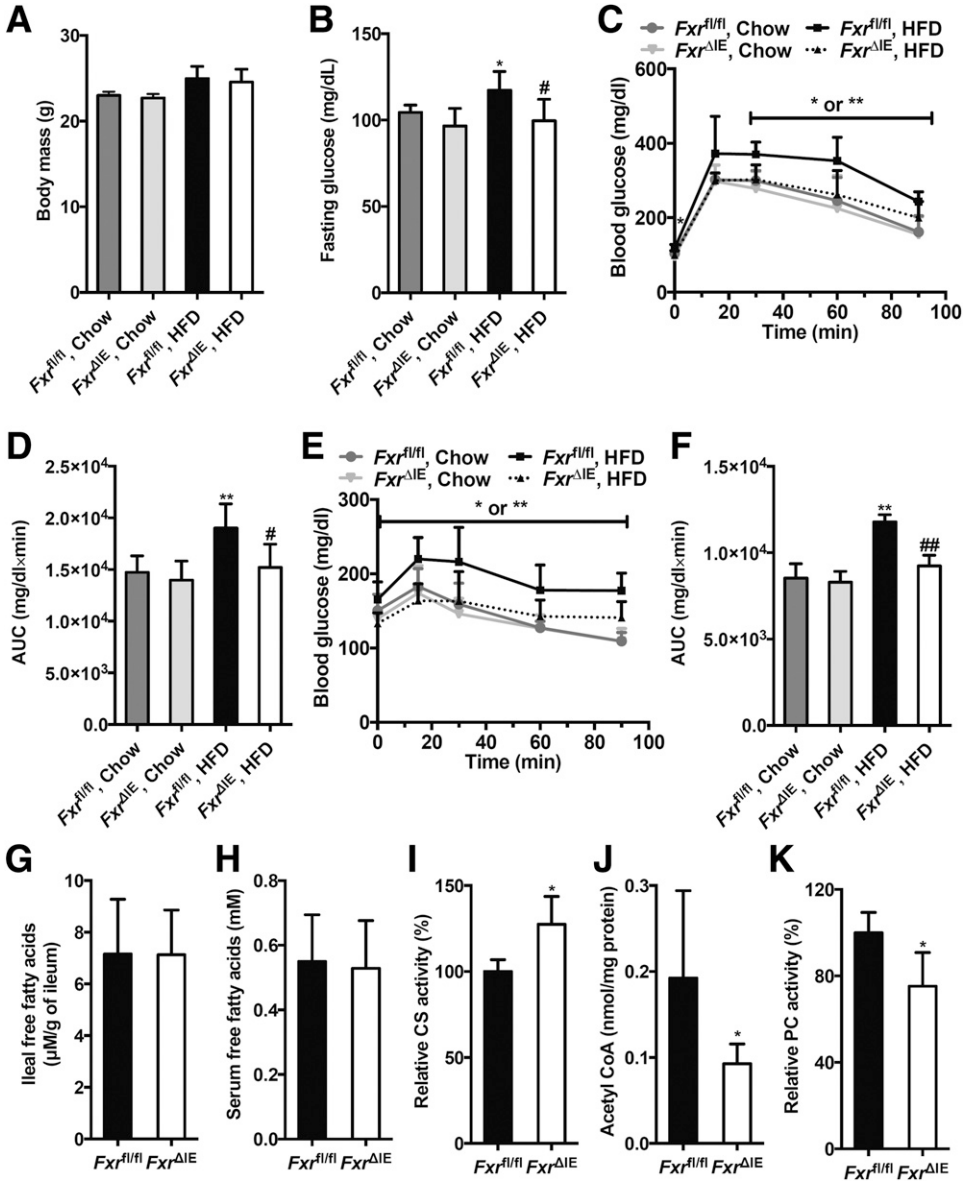

Figure 4—Inhibition of the intestinal FXR substantially decreases the hepatic gluconeogenesis by attenuating the hepatic mitochondrial acetyl-CoA levels and the hepatic PC activities independent of body weight changes. The $Fxr^{fl/fl}$ and $Fxr^{\Delta IE}$ mice were fed a chow diet or HFD for 1 week ($n = 7$). *A*: Body weights. *B*: Fasting plasma glucose levels. GTT (*C*) and area under the curve (AUC) (*D*). PTT (*E*) and AUC (*F*). The free fatty acid levels in ileum (*G*) and serum (*H*). *I*: The mitochondrial CS activities in the liver. *J*: The mitochondrial acetyl-CoA concentrations in the liver. *K*: The mitochondrial PC activities in the liver. Data are presented as the means ± SD. *A–F*: One-way ANOVA with Tukey correction: $^{*}P < 0.05$ and $^{**}P < 0.01$ vs. vehicle-treated $Fxr^{fl/fl}$ mice fed a chow diet; $\#P < 0.05$ and $\#\#P < 0.01$ vs. vehicle-treated $Fxr^{fl/fl}$ mice fed an HFD. *G–K*: Two-tailed Student *t* test: $^{*}P < 0.05$ vs. $Fxr^{fl/fl}$ mice.

Ceramide treatment inhibited *Cs* mRNA expression in primary hepatocytes in a dose-dependent manner (Fig. 8*A*). Similar results were also observed after treatment with the ER stress inducer thapsigargin (Fig. 8*A*). To investigate whether the induction of ER stress was responsible for the ceramide-inhibited *Cs* expression, the classic ER stress inhibitor TUDCA was used. Consistently, ceramide-elevated mRNA expression from the ER stress genes *Atf4*, *Atf6*, *Bip*, and *Chop* and calcium transport–related genes *Ip3r1* and *Ip3r2* was reversed after treatment with TUDCA both in vitro and in vivo (Fig. 8*B* and *C*). TUDCA markedly abolished the downregulation of *Cs* mRNA levels and mitochondrial CS activities in ceramide-treated primary hepatocytes and ceramide-treated mice, respectively (Fig. 8*D* and *E*). Hepatic mitochondrial acetyl-CoA levels and PC activities that were increased in ceramide-treated mice were decreased to similar levels in the vehicle group after administration of TUDCA (Fig. 8*F* and *G*). Furthermore, TUDCA stimulation substantially blunted elevated glucose production by ceramide treatment of primary hepatocytes (Fig. 8*H*). These results indicate that inhibition of the intestinal FXR-ceramide pathway

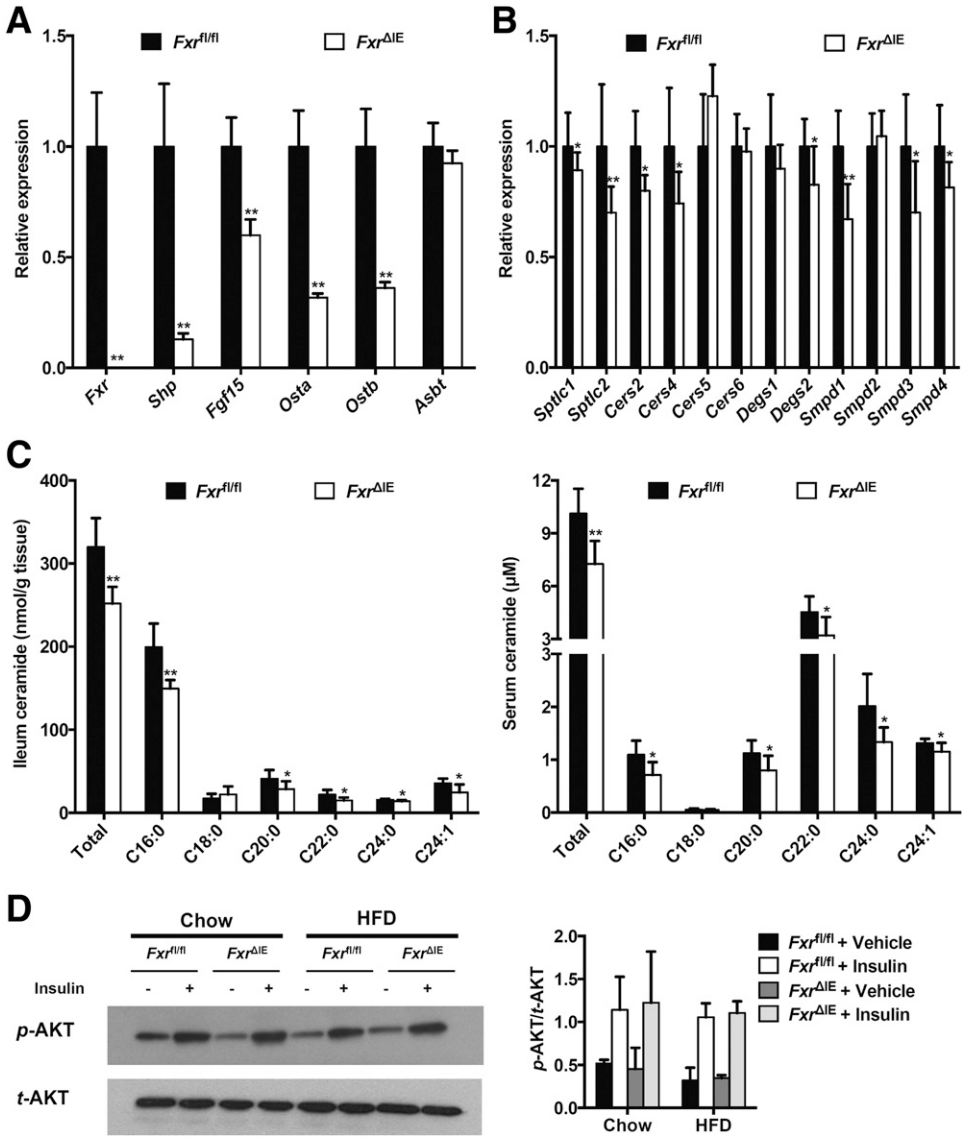

Figure 5—Inhibition of intestinal FXR substantially decreases hepatic gluconeogenesis independent of hepatic insulin signaling changes. The $Fxr^{fl/fl}$ and $Fxr^{\Delta IE}$ mice were fed an HFD or a chow diet for 1 week ($n = 7$). *A*: The mRNA levels of FXR target genes in the ileum. *B*: The mRNA levels of the ceramide synthesis-related genes in the ileum. *C*: The total and individual ceramide levels in the ileum (left) and serum (right). Data are presented as the means ± SD. Two-tailed Student *t* test: $^*P < 0.05$ and $^{**}P < 0.01$ vs. $Fxr^{fl/fl}$ mice. *D*: Western blot of insulin-stimulated AKT phosphorylation in the liver and quantitation of p-AKT/t-AKT ratios from three independent experiments.

increases hepatic mitochondrial CS activities and further reduces hepatic mitochondrial acetyl-CoA levels, PC activities, and hepatic gluconeogenesis by suppressing hepatic ER stress, ER-mitochondria tethering, and calcium transport.

DISCUSSION

The current study demonstrated that selective inhibition of intestinal FXR after administration of CAPE substantially downregulated hepatic gluconeogenesis by enhancing hepatic mitochondrial CS activities and then reducing hepatic mitochondrial acetyl-CoA levels and PC activities without affecting hepatic insulin signaling, mainly resulting from decreased intestine-derived ceramides (Supplementary Fig. 6). Further, ceramide administration markedly inhibited mitochondrial CS activity through the induction of hepatic ER stress, ER-mitochondria tethering, and calcium influx, which was primarily responsible for the increased hepatic mitochondrial acetyl-CoA levels and PC activity. Thus, the CAPE-inhibited intestinal FXR-ceramide pathway reduced hepatic mitochondrial acetyl-CoA levels and PC activity.

The role of FXR during the pathogenesis of metabolic dysfunctions might differ between the liver and intestine (15,16). In liver, FXR deficiency substantially increases gluconeogenesis, thus aggravating glucose intolerance and insulin resistance (17,18). Activation of hepatic FXR by GW4064 improved glucose tolerance

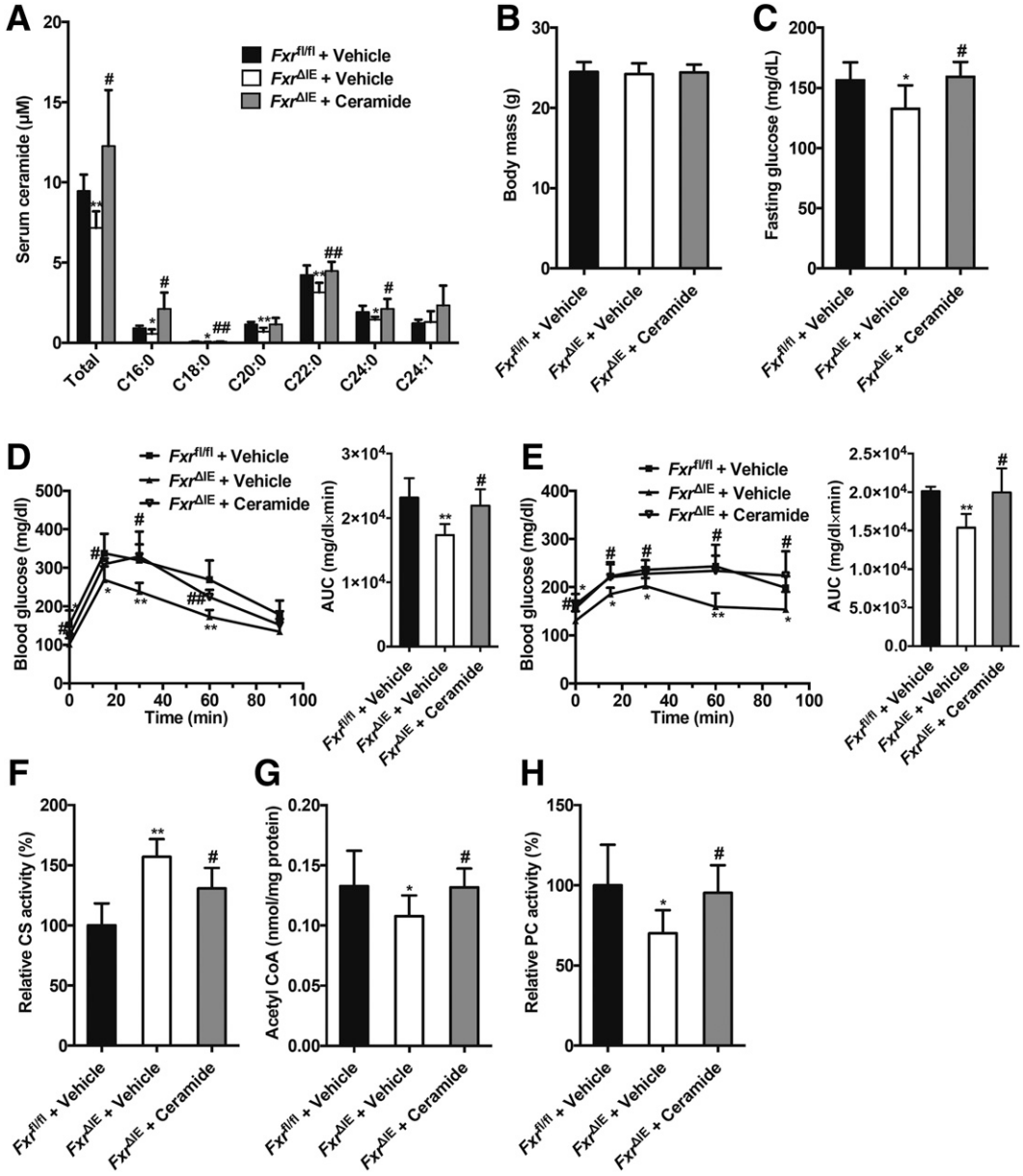

Figure 6—Administration of ceramide reverses the inhibition of hepatic mitochondrial acetyl-CoA levels and the hepatic PC activities by suppressing intestinal FXR signaling independent of body weight. The $Fxr^{fl/fl}$ and $Fxr^{\Delta IE}$ mice fed an HFD were injected with or without ceramide for 1 week (n = 7). *A*: The total and individual ceramide levels in the serum. *B*: Body weights. *C*: Fasting plasma glucose levels. *D*: GTT (left) and area under the curve (AUC) (right). *E*: PTT (left) and AUC (right). *F*: Mitochondrial CS activities in the liver. *G*: Mitochondrial acetyl-CoA concentrations in the liver. *H*: Mitochondrial PC activities in the liver. Data are presented as the means ± SD. One-way ANOVA with Tukey correction: $^{*}P < 0.05$ and $^{**}P < 0.01$ vs. vehicle-treated $Fxr^{fl/fl}$ mice; $\#P < 0.05$ and $\#\#P < 0.01$ vs. vehicle-treated $Fxr^{\Delta IE}$ mice.

and insulin resistance via downregulation of hepatic gluconeogenesis–related gene expression and increasing expression of glycogenesis-related genes (6). Obeticholic acid, which is a potent FXR agonist, has shown beneficial effects on hepatic steatosis and insulin sensitivity in both mice and humans (19–21). However, in the intestine, FXR activation impaired energy expenditure, and further aggravated obesity and glucose intolerance (22), whereas intestinal FXR inhibition exerted metabolic benefits (16,23). In the current study, GW4064 treatment at low dose, which is much lower than the dose known to activate liver FXR, can activate intestine FXR and promote hyperglycemia. CAPE treatment substantially inhibited hepatic gluconeogenesis and further improved glucose homeostasis by selectively suppressing intestinal FXR signaling. This is rather fortuitous since inhibition of hepatic FXR results in cholestasis, as previously reported (24). Mechanistically, intestinal FXR controls ceramide metabolism. Others reported that FXR activation in L cells of the intestine decreases glycolysis and ATP production, which, in turn, decreases proglucagon expression and GLP-1 secretion, and FXR deficiency in vivo increased

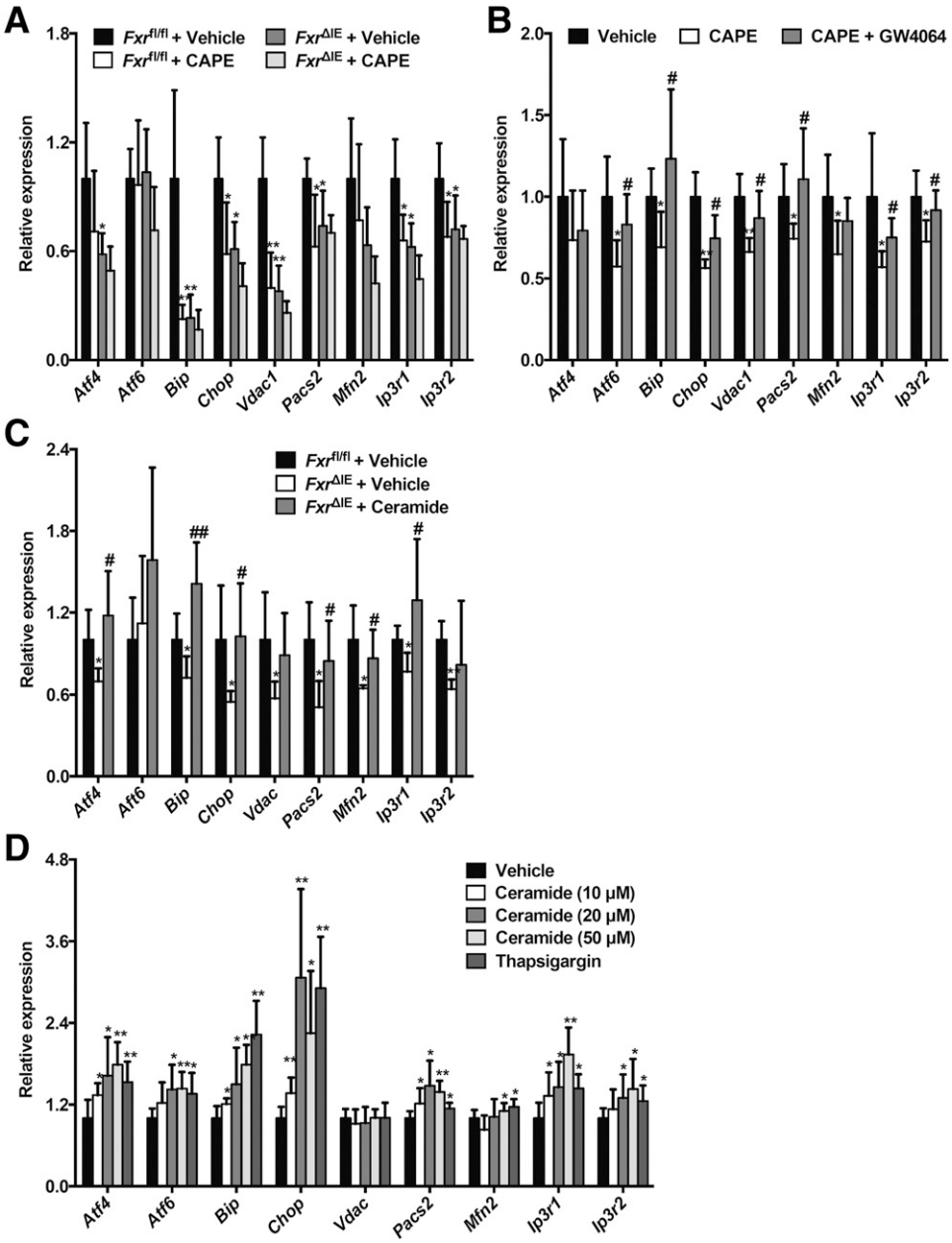

Figure 7—CAPE decreases ER stress and downregulates ER-mitochondria tethering and calcium transport through inhibition of ceramide synthesis. The mRNA levels of the ER stress–related genes, ER-mitochondria tethering–related genes, and calcium transport–related genes in the liver of the $Fxr^{fl/fl}$ mice and $Fxr^{\Delta IE}$ mice treated with or without CAPE for 4 weeks on an HFD (*A*); the vehicle-, CAPE-, and CAPE+GW4064–treated mice fed an HFD for 4 weeks (*B*); or the $Fxr^{fl/fl}$ mice and $Fxr^{\Delta IE}$ mice on an HFD treated with or without ceramide for 1 week (*C*). $n = 5$ or 7. One-way ANOVA with Tukey correction: $^{*}P < 0.05$ and $^{**}P < 0.01$ vs. vehicle-treated $Fxr^{fl/fl}$ mice (*A*); $^{*}P < 0.05$ and $^{**}P < 0.01$ vs. vehicle; $\#P < 0.05$ compared with the CAPE treatment (*B*); $^{*}P < 0.05$ and $^{**}P < 0.01$ vs. vehicle-treated $Fxr^{fl/fl}$ mice; $\#P < 0.05$ and $\#\#P < 0.01$ vs. vehicle-treated $Fxr^{\Delta IE}$ mice (*C*). *D*: The mRNA levels of the ER stress–related genes, ER-mitochondria tethering–related genes, and calcium transport–related genes in the primary hepatocytes after 8 h of ceramide or thapsigargin stimulation ($n = 6$). Two-tailed Student *t* test: $^{*}P < 0.05$ and $^{**}P < 0.01$ vs. vehicle. Data are presented as the means ± SD.

GLP-1 in response to glucose, hence improving glucose metabolism (25). Consistently, intestine FXR deficiency also increased serum GLP-1 levels (C.X., unpublished observations). However, the increased GLP-1 cannot affect the insulin production, as indicated by the unchanged levels of serum C-peptide, a marker of insulin production, and insulin levels after 1 week of HFD treatment. The physiological role of the FXR/GLP-1 pathway in insulin secretion in β-cells in long-term HFD-treated mice needs further investigation.

Ceramides, at high levels, induce obesity and insulin resistance (26), and deficiencies in ceramide synthase enzyme 6 (CERS6) markedly ameliorated HFD-induced obesity and insulin resistance mainly via reduced C16:0

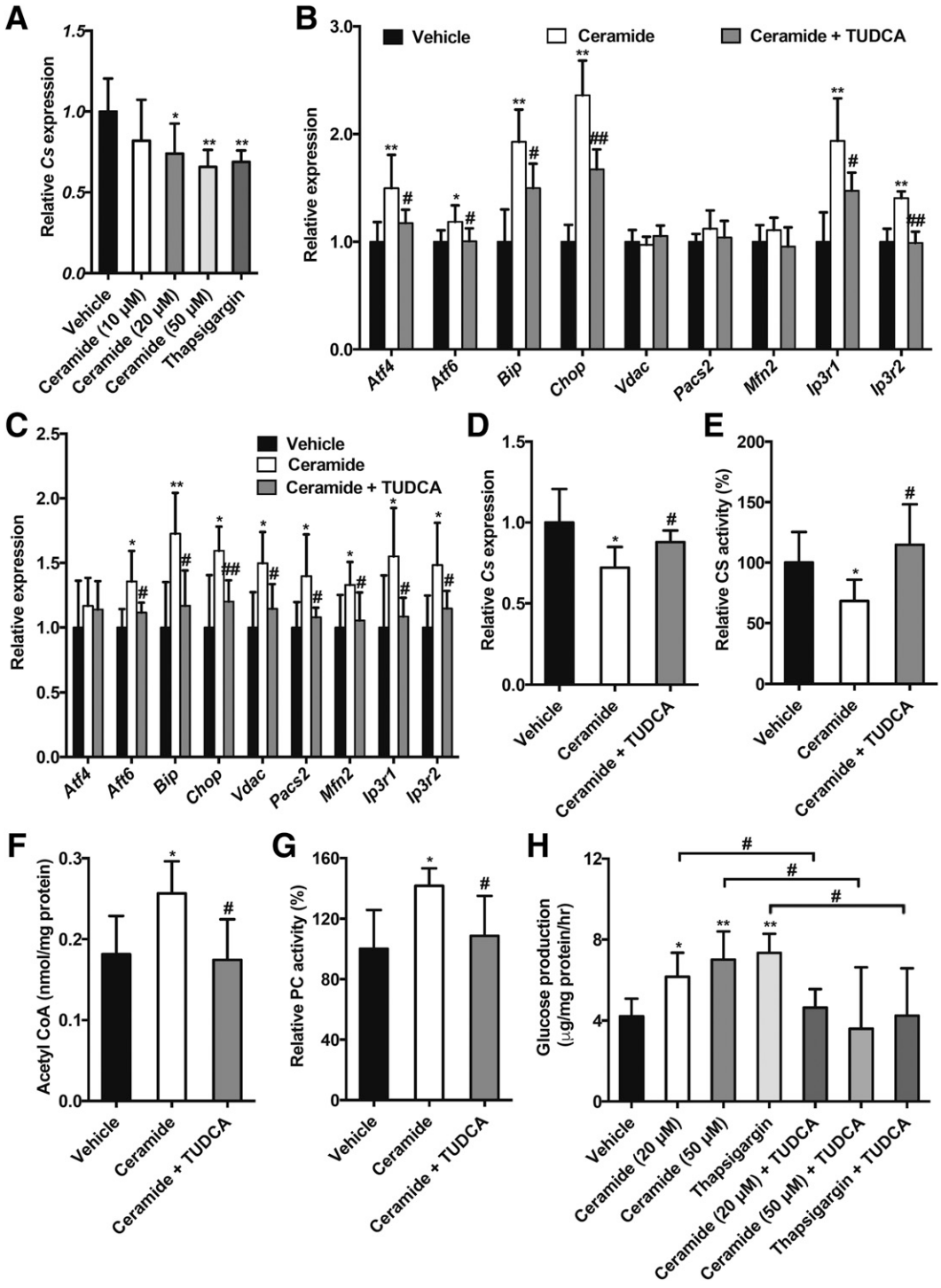

Figure 8—Ceramide decreases the *Cs* expression via induction of ER stress, ER-mitochondria tethering, and calcium transport. *A*: *Cs* expression in primary hepatocytes after 8 h of ceramide or thapsigargin stimulation (n = 6). Two-tailed Student t test: $^{*}P < 0.05$ and $^{**}P < 0.01$ vs. vehicle. *B*: The mRNA levels of the ER stress–related genes, ER-mitochondria tethering–related genes, and calcium transport–related genes in the primary hepatocytes. *C*: The mRNA levels of the ER stress–related genes, ER-mitochondria tethering–related genes, and calcium transport–related genes in the liver. *D*: The mRNA levels of *Cs* in the primary hepatocytes. *B* and *D*: The primary hepatocytes were exposed to ceramide and the ER stress inhibitor TUDCA for 8 h (n = 6). One-way ANOVA with Tukey correction: $^{*}P < 0.05$ and $^{**}P < 0.01$ vs. vehicle; $\#P < 0.05$ and $\#\#P < 0.01$ vs. ceramide treatment. The mitochondrial CS activities (*E*), mitochondrial acetyl-CoA levels (*F*), and mitochondrial PC activities (*G*) in the liver. *C* and *E*–*G*: Mice were fed an HFD for 1 week and treated with ceramide and TUDCA (n = 5). One-way ANOVA with Tukey correction: $^{*}P < 0.05$ and $^{**}P < 0.01$ vs. vehicle; $\#P < 0.05$ and $\#\#P < 0.01$ vs. ceramide treatment. *H*: Hepatic glucose production in the primary hepatocytes treated with ceramide, thapsigargin, and TUDCA (n = 6). One-way ANOVA with Tukey correction: $^{*}P < 0.05$ and $^{**}P < 0.01$ vs. vehicle; $\#P < 0.05$ vs. ceramide or thapsigargin treatment. Data are presented as the means ± SD.

ceramide levels (27), whereas CERS6 overexpression aggravated HFD-induced insulin resistance and hepatic steatosis (27,28). The overexpression of adipose or liver acid ceramidase, a ceramide degradation enzyme, decreases serum ceramide levels and improved hepatic steatosis and insulin resistance, respectively (29). Consistent with these findings, decreased intestinal-derived ceramide levels mediated attenuation of hepatic gluconeogenesis in $Fxr^{\Delta IE}$ mice as compared with $Fxr^{fl/fl}$ mice. Ceramide treatment disturbed glucose homeostasis via inhibition of insulin signaling caused by activation of the PKCζ pathway (30). Ceramides also induced pancreatic β-cell apoptosis and impaired insulin production in diabetes (31). However, serum C-peptide and insulin levels were not changed between $Fxr^{fl/fl}$ and $Fxr^{\Delta IE}$ mice fed an HFD for 1 week (C.X., unpublished observations). Moreover, hepatic insulin signaling was not changed in $Fxr^{\Delta IE}$ mice. These results suggested a minimal role for insulin secretion and hepatic insulin signaling in attenuating hepatic gluconeogenesis by inhibition of intestine FXR. The current study showed that ceramide induced hepatic ER stress and further increased ER-mitochondria tethering and calcium transport, thus leading to impaired mitochondrial CS activities. Ceramides further elevated hepatic mitochondrial acetyl-CoA levels, PC activities, and gluconeogenesis without affecting hepatic insulin signaling. Ceramides also impaired energy expenditures and induced obesity through hypothalamic ER stress (32). Obesity-triggered ER stress increased mitochondrial calcium influx mainly through excessive ER-mitochondria coupling in the liver, which could lead to hepatic metabolic abnormalities (14). In support of the present observation, calcium overload attenuated CS activities (33). Although it should be noted that there are other pathways influencing acetyl-CoA levels, such as fatty acid β-oxidation, ketogenesis, and de novo lipogenesis, expression of fatty acid β-oxidation genes is not altered (8), hepatic de novo lipogenesis is repressed (9), and the *Acaa1b* and *Hmgsc2* genes involved in ketogenesis are actually downregulated by FXR inhibition in the ileum (34). Thus, these alternative pathways would lead to either no change or an increase in hepatic acetyl-CoA levels, not the decreased levels seen in the current study.

Recent evidence suggests that increased hepatic acetyl-CoA levels mediated HFD-enhanced hepatic gluconeogenesis through activation of hepatic mitochondria PC independent of hepatic insulin signaling (4). This view is further supported by the finding that inhibition of intestinal FXR reduced HFD-induced hyperglycemia resulting from decreased hepatic acetyl-CoA levels. Others reported that the increased fatty acids derived from white adipose tissue lipolysis triggered the elevated acetyl-CoA contents in livers of mice fed an HFD (4). However, free fatty acid levels in both ileum and serum were not different between the $Fxr^{fl/fl}$ and $Fxr^{\Delta IE}$ mice fed an HFD. Interestingly, ceramide species were identified as novel lipids that regulate hepatic mitochondrial acetyl-CoA levels and PC activity mainly through modification of hepatic CS activity.

CAPE was reported to have many beneficial metabolic properties, such as antioxidant, anti-inflammatory, antiobesity, and antidiabetes activities (35,36). In the present work, CAPE inhibited hepatic gluconeogenesis and improved glucose metabolism deregulation by modulating the T-β-MCA–intestinal FXR–ceramide pathway. It should be noted that CAPE also has antibacterial effects through modification of reactive oxygen species signaling, indicating that CAPE could also modify the gut microbiota (36,37). Therefore, CAPE might indirectly inhibit BSH activity resulting from the modulation of gut microbiota; this possibility requires further investigation. In addition, it cannot be excluded that CAPE may have some effects on hepatic gluconeogenesis through non-FXR pathways, as CAPE treatment in wild-type mice tended to increase CS and PDH activity more in vehicle-treated $Fxr^{\Delta IE}$ mice, although it is not significant.

In conclusion, this study suggested that inhibition of intestine FXR signaling by administration of CAPE improved glucose metabolism dysfunction through the intestinal FXR-ceramide pathway, leading to decreased hepatic mitochondrial acetyl-CoA levels and PC activities without affecting hepatic insulin signaling. Thus, modification of bacterial bile acid metabolism by use of a BSH inhibitor may represent a promising therapeutic strategy to treat type 2 diabetes–associated hyperglycemia. However, it needs to be emphasized that there are significant differences between the mechanism of metabolic disease between humans and mice and that some of the findings in the current study may not be directly translatable to humans, in particular the interaction between the intestinal microbiota, bile acid metabolites, and intestinal FXR signaling (38). Furthermore, whether activation or inhibition of intestinal FXR will be of more benefit to the treatment of metabolic disease is an area of intense interest (38,39).

Funding. This work was supported by the Intramural Research Program, Center for Cancer Research, National Cancer Institute (ZIA BC005562 28), National Institutes of Health; the National Institutes of Environmental Health Sciences (ES022186 to A.D.P.); the National Key Research and Development Program of China (2016YFC0903100 and 2016YFC09031002); and the National Natural Science Foundation of China (81403007 and 81522007).

Duality of Interest. No potential conflicts of interest relevant to this article were reported by any of the authors.

Author Contributions. C.X. and C.J. designed, supervised, and performed the research; analyzed the data; and wrote the manuscript. J.S., X.G., D.S., L.S., T.W., S.T., M.A., and K.W.K. performed the research and analyzed the data. A.D.P. and F.J.G. designed and supervised the research and wrote the manuscript. F.J.G. is the guarantor of this work and, as such, had full access to all the data in the study and takes responsibility for the integrity of the data and the accuracy of the data analysis.

References

1. Sharabi K, Tavares CD, Rines AK, Puigserver P. Molecular pathophysiology of hepatic glucose production. Mol Aspects Med 2015;46:21–33
2. Kumashiro N, Beddow SA, Vatner DF, et al. Targeting pyruvate carboxylase reduces gluconeogenesis and adiposity and improves insulin resistance. Diabetes 2013;62:2183–2194
3. Pietrocola F, Galluzzi L, Bravo-San Pedro JM, Madeo F, Kroemer G. Acetyl coenzyme A: a central metabolite and second messenger. Cell Metab 2015;21:805–821
4. Perry RJ, Camporez JP, Kursawe R, et al. Hepatic acetyl CoA links adipose tissue inflammation to hepatic insulin resistance and type 2 diabetes. Cell 2015;160:745–758
5. de Aguiar Vallim TQ, Tarling EJ, Edwards PA. Pleiotropic roles of bile acids in metabolism. Cell Metab 2013;17:657–669
6. Zhang Y, Lee FY, Barrera G, et al. Activation of the nuclear receptor FXR improves hyperglycemia and hyperlipidemia in diabetic mice. Proc Natl Acad Sci U S A 2006;103:1006–1011
7. Sayin SI, Wahlström A, Felin J, et al. Gut microbiota regulates bile acid metabolism by reducing the levels of tauro-beta-muricholic acid, a naturally occurring FXR antagonist. Cell Metab 2013;17:225–235
8. Li F, Jiang C, Krausz KW, et al. Microbiome remodelling leads to inhibition of intestinal farnesoid X receptor signalling and decreased obesity. Nat Commun 2013;4:2384
9. Jiang C, Xie C, Li F, et al. Intestinal farnesoid X receptor signaling promotes nonalcoholic fatty liver disease. J Clin Invest 2015;125:386–402
10. Smith K, Zeng X, Lin J. Discovery of bile salt hydrolase inhibitors using an efficient high-throughput screening system. PLoS One 2014;9:e85344
11. Kim I, Ahn SH, Inagaki T, et al. Differential regulation of bile acid homeostasis by the farnesoid X receptor in liver and intestine. J Lipid Res 2007;48:2664–2672
12. Bezerra RM, Veiga LF, Caetano AC, et al. Caffeic acid phenethyl ester reduces the activation of the nuclear factor κB pathway by high-fat diet-induced obesity in mice. Metabolism 2012;61:1606–1614
13. Lee YS, Li P, Huh JY, et al. Inflammation is necessary for long-term but not short-term high-fat diet-induced insulin resistance. Diabetes 2011;60:2474–2483
14. Arruda AP, Pers BM, Parlakgül G, Güney E, Inouye K, Hotamisligil GS. Chronic enrichment of hepatic endoplasmic reticulum-mitochondria contact leads to mitochondrial dysfunction in obesity. Nat Med 2014;20:1427–1435
15. Prawitt J, Caron S, Staels B. Glucose-lowering effects of intestinal bile acid sequestration through enhancement of splanchnic glucose utilization. Trends Endocrinol Metab 2014;25:235–244
16. Jiang C, Xie C, Lv Y, et al. Intestine-selective farnesoid X receptor inhibition improves obesity-related metabolic dysfunction. Nat Commun 2015;6:10166
17. Ma K, Saha PK, Chan L, Moore DD. Farnesoid X receptor is essential for normal glucose homeostasis. J Clin Invest 2006;116:1102–1109
18. Cariou B, van Harmelen K, Duran-Sandoval D, et al. The farnesoid X receptor modulates adiposity and peripheral insulin sensitivity in mice. J Biol Chem 2006;281:11039–11049
19. Cipriani S, Mencarelli A, Palladino G, Fiorucci S. FXR activation reverses insulin resistance and lipid abnormalities and protects against liver steatosis in Zucker (fa/fa) obese rats. J Lipid Res 2010;51:771–784
20. Mudaliar S, Henry RR, Sanyal AJ, et al. Efficacy and safety of the farnesoid X receptor agonist obeticholic acid in patients with type 2 diabetes and nonalcoholic fatty liver disease. Gastroenterology 2013;145:574.e1–582.e1
21. Neuschwander-Tetri BA, Loomba R, Sanyal AJ, et al.; NASH Clinical Research Network. Farnesoid X nuclear receptor ligand obeticholic acid for noncirrhotic, non-alcoholic steatohepatitis (FLINT): a multicentre, randomised, placebo-controlled trial. Lancet 2015;385:956–965
22. Watanabe M, Horai Y, Houten SM, et al. Lowering bile acid pool size with a synthetic farnesoid X receptor (FXR) agonist induces obesity and diabetes through reduced energy expenditure. J Biol Chem 2011;286:26913–26920
23. Flynn CR, Albaugh VL, Cai S, et al. Bile diversion to the distal small intestine has comparable metabolic benefits to bariatric surgery. Nat Commun 2015;6:7715
24. Sinal CJ, Tohkin M, Miyata M, Ward JM, Lambert G, Gonzalez FJ. Targeted disruption of the nuclear receptor FXR/BAR impairs bile acid and lipid homeostasis. Cell 2000;102:731–744
25. Trabelsi MS, Daoudi M, Prawitt J, et al. Farnesoid X receptor inhibits glucagon-like peptide-1 production by enteroendocrine L cells. Nat Commun 2015;6:7629
26. Bikman BT, Summers SA. Ceramides as modulators of cellular and whole-body metabolism. J Clin Invest 2011;121:4222–4230
27. Turpin SM, Nicholls HT, Willmes DM, et al. Obesity-induced CerS6-dependent C16:0 ceramide production promotes weight gain and glucose intolerance. Cell Metab 2014;20:678–686
28. Raichur S, Wang ST, Chan PW, et al. CerS2 haploinsufficiency inhibits β-oxidation and confers susceptibility to diet-induced steatohepatitis and insulin resistance. [published correction appears in Cell Metab 2014;20:919]. Cell Metab 2014;20:687–695
29. Xia JY, Holland WL, Kusminski CM, et al. Targeted induction of ceramide degradation leads to improved systemic metabolism and reduced hepatic steatosis. Cell Metab 2015;22:266–278
30. Chavez JA, Summers SA. A ceramide-centric view of insulin resistance. Cell Metab 2012;15:585–594
31. Boslem E, Meikle PJ, Biden TJ. Roles of ceramide and sphingolipids in pancreatic β-cell function and dysfunction. Islets 2012;4:177–187
32. Contreras C, González-García I, Martínez-Sánchez N, et al. Central ceramide-induced hypothalamic lipotoxicity and ER stress regulate energy balance. Cell Reports 2014;9:366–377
33. Capel F, Demaison L, Maskouri F, et al. Calcium overload increases oxidative stress in old rat gastrocnemius muscle. J Physiol Pharmacol 2005;56:369–380
34. Zhang L, Xie C, Nichols RG, et al. Farnesoid X receptor signaling shapes the gut microbiota and controls hepatic lipid metabolism. mSystems 2016;1:e00070-16
35. Tolba MF, Omar HA, Azab SS, Khalifa AE, Abdel-Naim AB, Abdel-Rahman SZ. Caffeic acid phenethyl ester: a review of its antioxidant activity, protective effects against ischemia-reperfusion injury and drug adverse reactions. Crit Rev Food Sci Nutr 2016;56:2183–2190
36. Murtaza G, Karim S, Akram MR, et al. Caffeic acid phenethyl ester and therapeutic potentials. Biomed Res Int 2014;2014:145342
37. Akyol S, Ugurcu V, Altuntas A, Hasgul R, Cakmak O, Akyol O. Caffeic acid phenethyl ester as a protective agent against nephrotoxicity and/or oxidative kidney damage: a detailed systematic review. Scientific World Journal 2014;2014:561971
38. Gonzalez FJ, Jiang C, Patterson AD. An intestinal microbiota-farnesoid x receptor axis modulates metabolic disease. Gastroenterology 2016;151:845–859
39. Fang S, Suh JM, Reilly SM, et al. Intestinal FXR agonism promotes adipose tissue browning and reduces obesity and insulin resistance. Nat Med 2015;21:159–165